



HAL
open science

Prediction of stable nanoscale skyrmions in monolayer $\text{Fe}_{0.5}\text{GeTe}_2$

Dongzhe Li, Soumyajyoti Haldar, Leo Kollwitz, Hendrik Schrautzer, Moritz A
Goerzen, Stefan Heinze

► **To cite this version:**

Dongzhe Li, Soumyajyoti Haldar, Leo Kollwitz, Hendrik Schrautzer, Moritz A Goerzen, et al.. Prediction of stable nanoscale skyrmions in monolayer $\text{Fe}_{0.5}\text{GeTe}_2$. Physical Review B, 2024, 109 (22), pp.L220404. 10.1103/PhysRevB.109.L220404 . hal-04610069







HAL Id: hal-04610069

<https://hal.science/hal-04610069v1>

Submitted on 12 Jun 2024

HAL is a multi-disciplinary open access archive for the deposit and dissemination of scientific research documents, whether they are published or not. The documents may come from teaching and research institutions in France or abroad, or from public or private research centers.

L'archive ouverte pluridisciplinaire **HAL**, est destinée au dépôt et à la diffusion de documents scientifiques de niveau recherche, publiés ou non, émanant des établissements d'enseignement et de recherche français ou étrangers, des laboratoires publics ou privés.

Prediction of stable nanoscale skyrmions in monolayer Fe_5GeTe_2 Dongzhe Li ^{1,*}, Soumyajyoti Haldar ², Leo Kollwitz ², Hendrik Schrautzer ^{2,3},
Moritz A. Goerzen ² and Stefan Heinze ^{2,4}¹*CEMES, Université de Toulouse, CNRS, 29 rue Jeanne Marvig, F-31055 Toulouse, France*²*Institute of Theoretical Physics and Astrophysics, University of Kiel, Leibnizstrasse 15, 24098 Kiel, Germany*³*Science Institute and Faculty of Physical Sciences, University of Iceland, VR-III, 107 Reykjavík, Iceland*⁴*Kiel Nano, Surface, and Interface Science (KiNSIS), University of Kiel, 24118 Kiel, Germany*

(Received 31 January 2024; revised 19 April 2024; accepted 21 May 2024; published 10 June 2024)

Using first-principles calculations and atomistic spin simulations, we predict stable isolated skyrmions with a diameter below 10 nm in a monolayer of the two-dimensional van der Waals ferromagnet Fe_5GeTe_2 , a material of significant experimental interest. A very large Dzyaloshinskii-Moriya interaction (DMI) is observed due to the intrinsic broken inversion symmetry and strong spin-orbit coupling for monolayer Fe_5GeTe_2 . We show that the nearest-neighbor approximation, often used in the literature, fails to describe the DMI. The strong DMI together with moderate in-plane magnetocrystalline anisotropy energy allows to stabilize nanoscale skyrmions in out-of-plane magnetic fields above ≈ 2 T. The energy barriers of skyrmions in monolayer Fe_5GeTe_2 are comparable to those of state-of-the-art transition-metal ultrathin films. We further predict that these nanoscale skyrmions can be stable for hours at temperatures up to 20 K.

DOI: [10.1103/PhysRevB.109.L220404](https://doi.org/10.1103/PhysRevB.109.L220404)

Magnetic skyrmions—localized, stable spin textures with intriguing topological and dynamical properties—have emerged as a promising avenue to realize next-generation spintronics devices [1–6]. During the last ten years, the main focus of the community so far has been on skyrmions in bulk systems [7–9] and interface-based systems of ultrathin films [10–14] and multilayers [15–17]. Recently, magnetic skyrmions were discovered in atomically thin two-dimensional (2D) van der Waals (vdW) materials, providing an ideal playground to push skyrmion technology to the single-layer limit [18,19]. Stabilizing skyrmions in 2D magnets can avoid pinning by defects due to high-quality vdW interfaces and the possibility of easy control of magnetism via external stimuli.

The Dzyaloshinskii-Moriya interaction (DMI), which prefers a canting of the spins of adjacent magnetic atoms, is often recognized as the key ingredient in forming magnetic skyrmions. The DMI originates from spin-orbit coupling (SOC) and relies on broken inversion symmetry. However, most 2D magnets exhibit inversion symmetry, therefore, the DMI is suppressed. Several strategies have been proposed to achieve DMI by breaking inversion symmetry. These include the family of Janus vdW magnets [20–22], electric field [23], and 2D vdW heterostructures [24–26]. In particular, the Fe_nGeTe_2 family ($n = 3, 4, 5$) with high Curie temperature (T_c) near room temperature has been proposed as a promising candidate for magnetic skyrmions. Néel-type magnetic skyrmions are reported in Fe_3GeTe_2 heterostructures by experiments [24–27] and explained by *ab initio* theory [28,29] in terms of the emergence of DMI at the interface. All-electrical

skyrmion detection has also recently been proposed in tunnel junctions based on Fe_3GeTe_2 [30]. More recently, several experimental groups reported the observation of topological spin structures (i.e., skyrmions or merons) and magnetic bubbles in 2D vdW Fe_5GeTe_2 [31–36]. Additionally, Fe_5GeTe_2 exhibits high T_c above room temperature [37,38], which makes it promising for spintronics device applications. However, the quantification of individual skyrmions' stability and lifetime in Fe_5GeTe_2 , crucial for device applications, has been reported neither in experiments nor in theory.

In this Letter, we predict the formation of nanoscale skyrmions in the atom-thick vdW Fe_5GeTe_2 monolayer based on first-principles calculations and atomistic spin simulations. The diameters of these skyrmions are below 10 nm, which is technologically desirable for improving the controllability and integrability of skyrmion-based functional devices. However, such small skyrmions have not yet been observed in 2D vdW magnets. The origin of these nanoscale skyrmions is attributed to strong DMI together with moderate in-plane magnetocrystalline anisotropy energy (MAE) and weak exchange frustration. Furthermore, the calculated energy barriers of skyrmion collapse for monolayer Fe_5GeTe_2 are ~ 80 meV at a moderate magnetic field of about 2 T. This substantial energy barrier is comparable to that of ultrathin films [39–41], which serve as prototype systems for hosting nanoscale skyrmions. Finally, we also calculate explicitly skyrmion lifetime as a function of magnetic field and temperature. Our results demonstrate that the Fe_5GeTe_2 monolayer is an excellent candidate to experimentally observe nanoscale skyrmions in a 2D vdW magnet.

Our first-principles calculations were performed using the FLEUR code [42] based on the full-potential linearized augmented plane wave method (see the Supplemental Material

*Corresponding author: dongzhe.li@cemes.fr

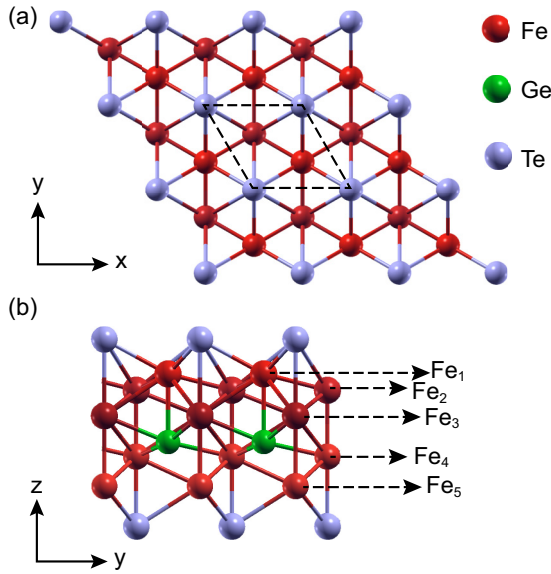


FIG. 1. (a) Top and (b) side views of the atomic structure of the Fe_5GeTe_2 monolayer. The black dashed lines draw up the 2D primitive cell.

for computational details [43]). We have calculated the energy dispersions $E(\mathbf{q})$ of flat spin spiral states [44,45] for the Fe_5GeTe_2 monolayer. A magnetic moment \mathbf{m}_i at atom position \mathbf{R}_i for a flat spin spiral is given by $\mathbf{m}_i = M[\cos(\mathbf{q} \cdot \mathbf{R}_i), \sin(\mathbf{q} \cdot \mathbf{R}_i), 0]$, with M denoting the size of the magnetic moment.

To determine the interactions of magnetic moments for the Fe_5GeTe_2 monolayer, we adopt the following atomistic spin Hamiltonian, which is fitted from spin spiral calculations without and with SOC

$$H = - \sum_{ij} J_{ij}(\mathbf{m}_i \cdot \mathbf{m}_j) - \sum_{ij} \mathbf{D}_{ij} \cdot (\mathbf{m}_i \times \mathbf{m}_j) + \sum_i K(m_i^z)^2 - \sum_i M(\mathbf{m}_i \cdot \mathbf{B}), \quad (1)$$

where \mathbf{m}_i and \mathbf{m}_j are normalized magnetic moments at position \mathbf{R}_i and \mathbf{R}_j , respectively. The four magnetic interaction terms correspond to the Heisenberg isotropic exchange, the DMI, the MAE, and the external magnetic field, and they are characterized by the interaction constants J_{ij} , \mathbf{D}_{ij} , and K , and B , respectively. Note that our spin model is adapted to a collective 2D model by treating five Fe layers of Fe_5GeTe_2 as a whole system, similar to a monolayer system. All magnetic interaction parameters are measured in meV/unit cell (uc).

We consider a Fe_5GeTe_2 monolayer where one Fe_1 is situated above Ge as shown in Fig. 1(a), the so-called UUU configuration. The calculated lattice constant is about 3.96 Å, which agrees well with previous results [46]. We are aware that there are two possible configurations for monolayer Fe_5GeTe_2 , namely UUU and UDU configurations [47,48]. In this work, we focus on the UUU configuration since skyrmionic spin structures are experimentally observed in this configuration [31,32]. For both spin channels, Fe_5GeTe_2 exhibits a metallic property (see Fig. S1 in the Supplemental Material [43]). The calculated spin moments are $-0.21\mu_B$,

$2.21\mu_B$, $1.70\mu_B$, $1.28\mu_B$, and $2.41\mu_B$ for the Fe_1 , Fe_2 , Fe_3 , Fe_4 , and Fe_5 atoms, respectively. Note that the calculated spin moments are, in general, in good agreement with previous *ab initio* results, as summarized in detail in Table S2 in the Supplemental Material [43]. It is important to note that the spin moment on Fe_1 is significantly quenched, which is also in good agreement with dynamical mean-field (DMFT) results [48].

We focus first on spin spiral calculations without SOC along the $\bar{M}\text{-}\bar{\Gamma}\text{-}\bar{K}\text{-}\bar{M}$ high-symmetry direction [Fig. 2(a)]. From the fitted parameters shown in Table I, we find the Heisenberg exchange to be largely dominated by the nearest neighbor contribution. This is also clearly seen from the fitted curve using only the nearest neighbor (NN) term [see dotted line in Fig. 2(a)]. On the other hand, exchange constants up to seventh neighbors (Table I) are necessary to fit the DFT results accurately [solid line in Fig. 2(a)]. Without SOC, the energy dispersion shows a minimum at the $\bar{\Gamma}$ point, which represents the ferromagnetic (FM) state. The energy difference between the $\bar{\Gamma}$ and the \bar{M} point [row-wise antiferromagnetic (AFM) state] is found to be about 137 meV for five Fe atoms. This energy difference is much smaller than that in the Fe_3GeTe_2 or Fe_4GeTe_2 monolayers (see Fig. S2 in the Supplemental Material [43]), leading to much smaller J_1 values (see Table I in the Supplemental Material [43]). We also note that the spin moment variation is mainly from Fe_1 and Fe_4 atoms (Fig. S3a in the Supplemental Material [43]). Additionally, we have also carefully checked the effect of variation of spin moments for our spin model by calculating conical spin spirals (see Sec. II, Fig. S3b, and Fig. S4 in the Supplemental Material [43].)

When SOC is taken into account, the DMI arises due to broken inversion symmetry. The Fe_5GeTe_2 monolayer favors cycloidal spin spirals with a counter-clockwise (CCW) rotational sense, as seen from the calculated energy contribution to the dispersion due to SOC, $\Delta E_{\text{SOC}}(\mathbf{q})$ [Fig. 2(b)]. If we apply the NN approximation, we obtain the effective DMI constant $D_{\text{eff}} = -0.88$ meV, and the corresponding micro-magnetic DMI is given by $D = \frac{3\sqrt{2}D_{\text{eff}}}{N_F a^2}$ (a and N_F are the lattice constant and the number of ferromagnetic layers). For the Fe_5GeTe_2 monolayer, the value is approximately 0.76 mJ/m², which is in reasonable agreement with the one calculated by the supercell approach ($\sim 0.48 - 0.67$ mJ/m²) [31] based on the NN approximation. However, as clearly seen in Fig. 2(b), the dashed lines with an effective NN DMI fail to capture our DFT results beyond the regime of small $|\mathbf{q}|$. The inclusion of interactions up to the seventh NN is needed to reproduce the DFT data accurately, and this is also reflected in the fitted parameters presented in Table I. The second NN interaction is on the same order of magnitude compared to the first NN one.

Additionally, SOC also introduces MAE. We find the easy magnetization axis of the Fe_5GeTe_2 monolayer to be in-plane with a MAE of 0.38 meV/uc. As observed in Fig. 2(c), a spin spiral energy minimum of -0.1 meV/uc compared to the FM state occurs in the $\bar{\Gamma}\bar{K}$ direction, which corresponds to a spin spiral period of $\lambda = 2\pi/|\mathbf{q}| = 19.9$ nm.

Including all interactions, i.e., Heisenberg exchange, DMI, and MAE, results in the spin spiral energy dispersion shown in Fig. 2(c). The energy contribution from the MAE leads to an energy offset of $K/2$ for spin spirals with a long

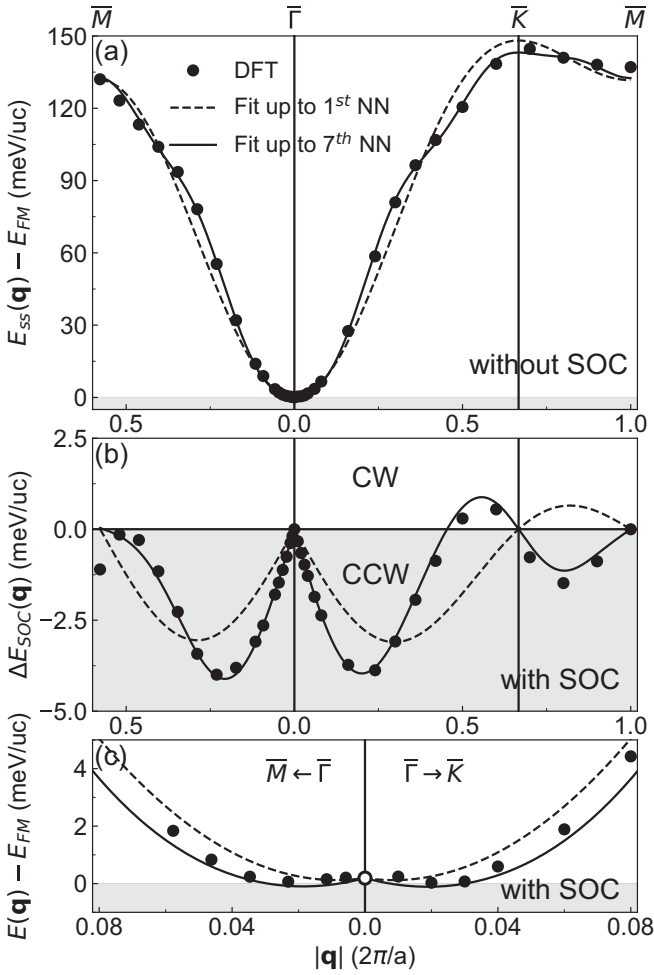


FIG. 2. (a) Energy dispersion of flat spin spirals (E_{SS}) for Fe_5GeTe_2 along the high symmetry path $\bar{M}-\bar{\Gamma}-\bar{K}-\bar{M}$ without SOC. The symbols represent the DFT calculations in scalar-relativistic approximation, while the dashed and solid lines are the fits to the Heisenberg exchange interaction up to the first nearest neighbor (NN) and up to the seventh NN, respectively. (b) Energy contribution of cycloidal spin spirals due to SOC (ΔE_{SOC}), also known as DMI contribution. All energies are measured with respect to the FM state (E_{FM}) at the $\bar{\Gamma}$ point. Note that positive and negative energies represent a preference for clockwise (CW) and counterclockwise (CCW) spin configurations. (c) Zoom around the FM state ($\bar{\Gamma}$ point), including the Heisenberg exchange, the DMI, and the MAE, i.e., $E(\mathbf{q}) = E_{SS}(\mathbf{q}) + \Delta E_{SOC}(\mathbf{q}) + K/2$. The DMI leads to a CCW rotational sense, and the MAE is responsible for the constant energy shift ($K/2$) of the spin spirals with respect to the FM state.

TABLE I. Full model: Shell-resolved Heisenberg exchange constants (J_i) and DMI constants (D_i) obtained by fitting the energy contribution to spin spirals without and with SOC, and spin moments (m_s) from DFT calculations as presented in Fig. 2 for the Fe_5GeTe_2 monolayer. Effective model: Parameters of the effective NN exchange and DMI model obtained by fitting the DFT results. A positive (negative) sign represents FM (AFM) coupling. A positive (negative) sign of D_i denotes a preference for CW (CCW) rotating cycloidal spin spirals. The Fe_5GeTe_2 monolayer favors in-plane MAE (i.e., $K > 0$). Note that all parameters are treated as a collective 2D spin model in a hexagonal symmetry (i.e., five Fe atoms in the supercell are treated as a whole). The magnetic moments are given in μ_B /unit cell (uc), and other parameters in meV/uc.

	J_1/J_{eff}	J_2	J_3	J_4	J_5	J_6	J_7	D_1/D_{eff}	D_2	D_3	D_4	D_5	D_6	D_7	K	m_s
Full model	14.803	0.898	0.466	0.916	0.231	-0.443	-0.599	-0.659	-0.523	-0.083	0.020	-0.008	-0.021	-0.008	0.380	7.306
Effective model	16.457							-0.880							0.380	7.306

period, i.e., small value of $|\mathbf{q}|$, with respect to the FM state, as can be seen in a zoom of $E(\mathbf{q})$ around $\bar{\Gamma}$. Interestingly, the ground state within the NN approximation is the FM state, while it is the spin spiral state when we include interactions up to the seventh NN. It is worth emphasizing that the spin spiral curve becomes extremely flat near the $\bar{\Gamma}$ point. It has been demonstrated that a flat energy dispersion around $\bar{\Gamma}$ is beneficial for stabilizing nanoscale skyrmions in ultrathin films [14]. To check the validity of our 2D collective spin model, we performed Monte-Carlo simulations (see Sec. III in the Supplemental Material [43]) with magnetic interaction parameters from the full model presented in Table I. We obtain the Curie temperature (T_c) of about 451 K (see Fig. S5 in the Supplemental Material [43]), which is in reasonable agreement with the value of $T_c = 390$ K obtained in Ref. [47].

To check the possibility of stabilizing nanoscale magnetic skyrmions in Fe_5GeTe_2 , we performed atomistic spin simulations using the spin model described by Eq. (1) with the full set of DFT parameters. We apply atomistic spin-dynamics via the Landau-Lifshitz equation to obtain isolated magnetic skyrmions. Minimum energy paths between the initial skyrmion and final FM state were calculated using the geodesic nudged elastic band (GNEB) method [49]. The energy barriers stabilizing skyrmions against collapse were obtained from the saddle point along this path. Finally, we used harmonic transition-state theory to quantify skyrmion stability by calculating their lifetime [40,50–52] (see the Supplemental Material for computational details [43]).

We create isolated skyrmions in the field-polarized background with an out-of-plane magnetization direction due to an applied magnetic field and fully relax these spin structures by solving the damped Landau-Lifshitz equation self-consistently. The in-plane FM state (denoted as FM_{\parallel}) exhibits slightly lower energy compared to the out-of-plane FM state, owing to the in-plane MAE of Fe_5GeTe_2 (see Fig. S6 in the Supplemental Material [43]). At zero magnetic field, we do not observe the emergence of skyrmions. Instead, we observe labyrinth domains with chiral Néel domain walls, which hold the lowest energy state. As we gradually increase the magnetic field B perpendicular to the monolayer, the labyrinthine domain shrinks and eventually vanishes, giving rise to isolated magnetic skyrmions at a critical field of $B_c = 2.2$ T. Note, that for fields above $B = 2K/M \approx 1.8$ T applied perpendicular to the film, the Zeeman energy exceeds the MAE [53].

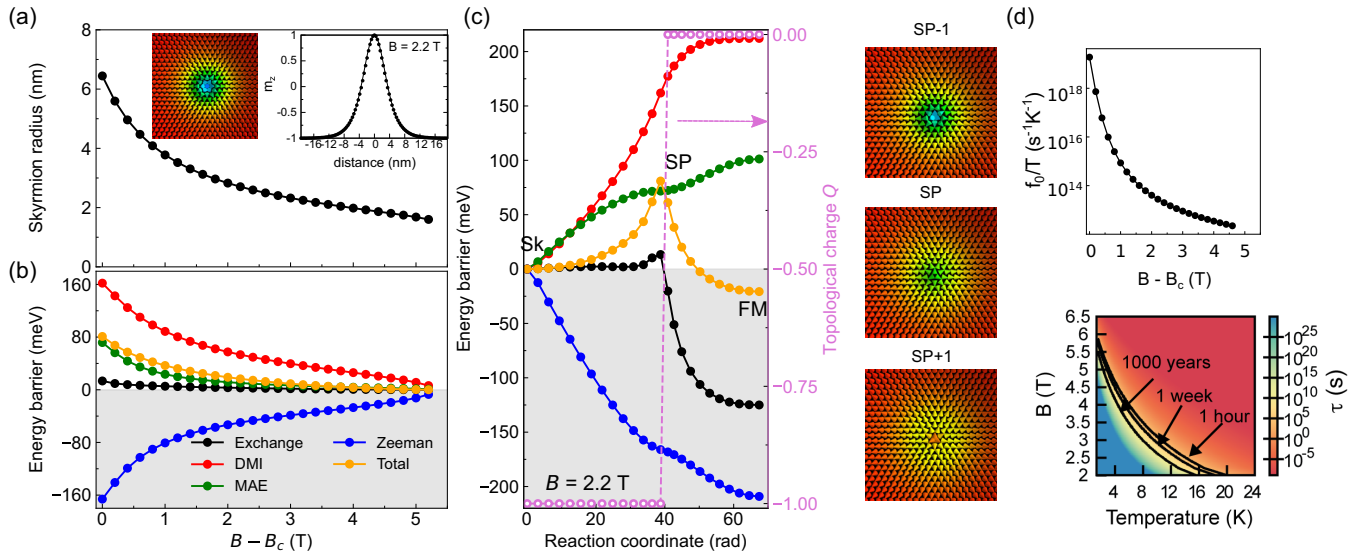


FIG. 3. Skyrmion radius and energy barrier for skyrmion collapse in the Fe_5GeTe_2 monolayer evaluated using magnetic interaction parameters from DFT. (a) Skyrmion radius as a function of $B - B_c$ where B_c is the critical field for stabilizing metastable magnetic skyrmions. The calculated value is $B_c = 2.2$ T for Fe_5GeTe_2 . The skyrmion profile and spin texture at $B = 2.2$ T are shown as insets. (b) Total energy barriers and their decomposition (see legend) of isolated skyrmions versus $B - B_c$. (c) Energy contributions from the different interactions [the same legend as in panel (b), left axis] are shown versus the reaction coordinate along the minimum energy path from the initial (skyrmion) state to the final (FM) state through the saddle point (SP). The energies are summed over all atoms of the simulation box and are given relative to the energies of the initial isolated skyrmion state. The topological charge (open circles, right axis) is plotted versus the reaction coordinate. (c) Corresponding spin structures before (SP-1), after (SP+1), and at the saddle point (SP) are shown. Note that the skyrmion collapse occurs via radially symmetrical shrinking. (d) Calculated attempt frequencies f_0 on a logarithmic scale with respect to $B - B_c$ (top panel). Skyrmion lifetimes of Fe_5GeTe_2 obtained in harmonic transition state theory based on the spin model with DFT parameters as a function of magnetic field and temperature (bottom panel).

Our atomistic spin simulations predict Néel-type magnetic skyrmions stabilized in the FM background [(see the inset of Fig. 3(a) for skyrmion profile and spin texture at $B = 2.2$ T)]. As expected, the skyrmion size decreases in Fe_5GeTe_2 with increasing magnetic field [Fig. 3(a)]. Interestingly, nanoscale skyrmions occur with a radius below 6.4 nm at $B > 2.2$ T, and isolated skyrmions can be obtained. Note that the skyrmion radius is estimated using the Bocdanov- Θ profile [54] within a wide range of $B = 2.2 \sim 7.6$ T. At $B > 7.6$ T, skyrmions collapse into the FM state.

To provide insight into skyrmion stability in monolayer Fe_5GeTe_2 , we show in Fig. 3(b) the calculated energy barriers protecting skyrmions from collapsing into the FM state with respect to $B - B_c$. Remarkably, we obtain an energy barrier of more than 80 meV at the critical field $B_c = 2.2$ T. This value is comparable to state-of-the-art ultrathin films that serve as prototype systems to host nanoscale skyrmions [39–41]. Note, that previous work on skyrmion stability in 2D magnets [28] reported smaller values than those found here for the Fe_5GeTe_2 monolayer.

From the energy decomposition of the barrier, we conclude that the DMI and MAE are mainly responsible for the skyrmion stability [Fig. 3(b)]. We also note that the energy barrier can be enhanced if we increase the in-plane MAE, a quantity that can be easily tuned in experiments by doping or temperature [55–57]. However, if the in-plane MAE is increased, larger magnetic fields are needed to obtain the field-polarized phase in which skyrmions can be stabilized.

To obtain information about transition mechanisms from the skyrmion state to the FM state via the saddle point (SP), which determines the barrier, we show in Fig. 3(c) the decomposition of the energy along the minimum energy path for skyrmion collapse at $B = 2.2$ T. The topological charge, calculated by $Q = \int \mathbf{m} \cdot (\frac{\partial \mathbf{m}}{\partial x} \times \frac{\partial \mathbf{m}}{\partial y}) dx dy$, changes from -1 to 0 at the SP. The skyrmion is annihilated via the radial symmetric collapse mechanism in which the skyrmion shrinks symmetrically to SP and then collapses into the FM state [52]. Again, it is clear that the DMI and MAE prefer the skyrmion (Sk) state and decrease the total barrier, while the Zeeman term strongly favors the FM state. Due to frustration, the Heisenberg exchange energy gives a small positive annihilation barrier.

The stability of metastable magnetic skyrmions can be quantified by their mean lifetime, τ , which is given by the Arrhenius law $\tau = f_0^{-1} \exp(\frac{\Delta E}{k_B T})$, where ΔE , f_0 , and T are energy barrier, attempt frequency, and temperature, respectively. The calculated f_0 within harmonic transition state theory [50] is shown in Fig. 3(d). As expected, f_0 depends strongly on the magnetic field. This effect is similar to that observed in ultrathin transition-metal films, which can be traced back to a change of entropy with skyrmion radius and profile [51,58]. From the temperature and field dependence of the skyrmion lifetime [Fig. 3(d)], we predict that isolated skyrmions in the Fe_5GeTe_2 are stable up to hours at a temperature at about 20 K and $B = 2.2$ T. Therefore, these nanoscale skyrmions can be probed by experiments using current state-of-the-art techniques, e.g., spin-polarized

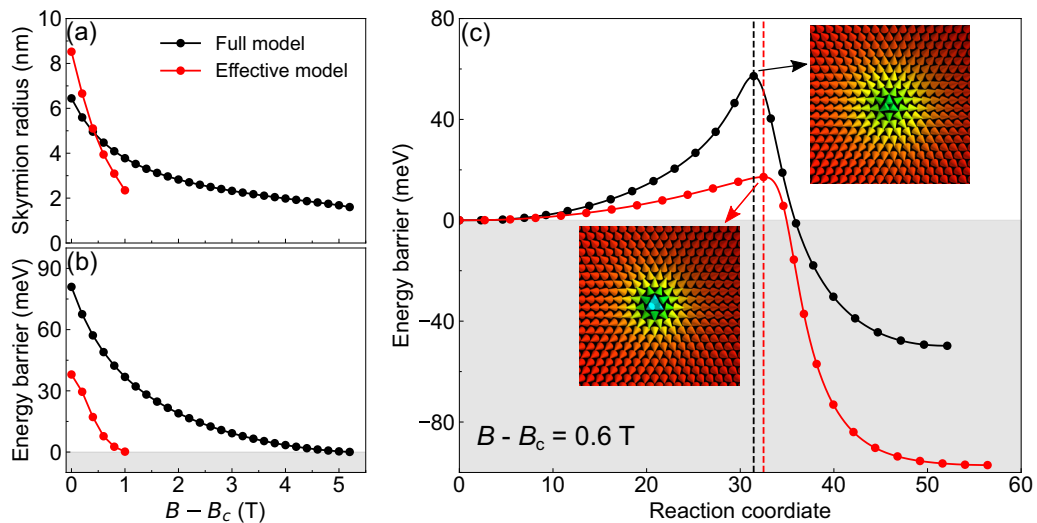


FIG. 4. Full model versus effective model comparison. (a) Skyrmion radius vs magnetic field. (b) Skyrmion energy barriers with respect to B . The estimated critical magnetic fields B_c are 2.2 T and 1.4 T for the full model and effective model, respectively. (c) Minimum energy paths of skyrmion collapse: Energies of the spin configurations during a skyrmion collapse are shown over the reaction coordinate corresponding to the progress of the collapse at $B - B_c = 0.6$ T. Our simulations were conducted using both the effective exchange model (in red) and considering all magnetic interactions from the DFT calculation (in black).

scanning tunneling microscopy or Lorentz transmission electron microscopy.

We plot in Fig. 4 the comparison of atomistic spin simulation results from parameters with the full and effective models. The critical magnetic field is found to be about 1.4 T in the case of the effective model, which is 0.8 T smaller than the one for the full model. In both models, we have sub-10 nm radius skyrmions [Fig. 4(a)] and energy barriers of a few 10 meV [Fig. 4(b)]. From the GNEB calculation at $B - B_c = 0.6$ T, the energy barriers for the full and effective models are rather different. We find a more than three times larger energy barrier with the full model, indicating the importance of including full magnetic parameters for the Fe_5GeTe_2 monolayer.

In summary, we propose, based on first-principles calculations and atomistic spin simulations, that monolayer Fe_5GeTe_2 is a compelling 2D vdW magnet with skyrmionic physics. Due to the large DMI together with moderate in-plane MAE, the Fe_5GeTe_2 monolayer can exhibit metastable nanoscale (sub-10 nm) skyrmions in an out-of-plane magnetic field above 2.2 T. We also highlight the importance of

including beyond nearest neighbor DMI terms in the atomistic spin model. The energy barriers protecting skyrmions against collapse are up to 80 meV, which are comparable to those of state-of-the-art transition-metal ultrathin films. Using harmonic transition-state theory, we predict that nanoscale skyrmions are stable in monolayer Fe_5GeTe_2 with lifetimes of hours up to 20 K.

This study has been supported through the ANR Grant No. ANR-22-CE24-0019. This study has been (partially) supported through the Grant NanoX No. ANR-17-EURE-0009 in the framework of the ‘‘Programme des Investissements d’Avenir’’. We gratefully acknowledge financial support from the Deutsche Forschungsgemeinschaft (DFG, German Research Foundation) through SPP2137 ‘‘Skyrmionics’’ (Project No. 462602351). H.S. would like to acknowledge financial support from the Icelandic Research Fund (Grant No. 239435). This work was performed using HPC resources from CALMIP (Grant No. 2021/2023-[P21023]), the North German Supercomputing Alliance (HLRN), and the Kiel University Computing Centre.

- [1] A. Fert, N. Reyren, and V. Cros, Magnetic skyrmions: Advances in physics and potential applications, *Nat. Rev. Mater.* **2**, 17031 (2017).
- [2] K. Everschor-Sitte, J. Masell, R. Reeve, and M. Kläui, Perspective: Magnetic skyrmions—overview of recent progress in an active research field, *J. Appl. Phys.* **124**, 240901 (2018).
- [3] S. Luo, M. Song, X. Li, Y. Zhang, J. Hong, X. Yang, X. Zou, N. Xu, and L. You, Reconfigurable skyrmion logic gates, *Nano Lett.* **18**, 1180 (2018).
- [4] B. Göbel, I. Mertig, and O. Tretiakov, Beyond skyrmions: Review and perspectives of alternative magnetic quasiparticles, *Phys. Rep.* **895**, 1 (2021).
- [5] S. Li, W. Kang, X. Zhang, T. Nie, Y. Zhou, K. Wang, and W. Zhao, Magnetic skyrmions for unconventional computing, *Mater. Horiz.* **8**, 854 (2021).
- [6] C. Psaroudaki and C. Panagopoulos, Skyrmion qubits: A new class of quantum logic elements based on nanoscale magnetization, *Phys. Rev. Lett.* **127**, 067201 (2021).
- [7] S. Mühlbauer, B. Binz, F. Jonietz, C. Pfleiderer, A. Rosch, A. Neubauer, R. Georgii, and P. Boni, Skyrmion lattice in a chiral magnet, *Science* **323**, 915 (2009).
- [8] X. Yu, N. Kanazawa, Y. Onose, K. Kimoto, W. Zhang, S. Ishiwata, Y. Matsui, and Y. Tokura, Near room-temperature

- formation of a skyrmion crystal in thin-films of the helimagnet FeGe, *Nat. Mater.* **10**, 106 (2011).
- [9] J. H. Yang, Z. L. Li, X. Z. Lu, M.-H. Whangbo, S.-H. Wei, X. G. Gong, and H. J. Xiang, Strong Dzyaloshinskii-Moriya interaction and origin of ferroelectricity in Cu_2OSe_3 , *Phys. Rev. Lett.* **109**, 107203 (2012).
- [10] S. Heinze, K. von Bergmann, M. Menzel, J. Brede, A. Kubetzka, R. Wiesendanger, G. Bihlmayer, and S. Blügel, Spontaneous atomic-scale magnetic skyrmion lattice in two dimensions, *Nat. Phys.* **7**, 713 (2011).
- [11] N. Romming, C. Hanneken, M. Menzel, J. Bickel, B. Wolter, K. von Bergmann, A. Kubetzka, and R. Wiesendanger, Writing and deleting single magnetic skyrmions, *Science* **341**, 636 (2013).
- [12] B. Dupé, M. Hoffmann, C. Paillard, and S. Heinze, Tailoring magnetic skyrmions in ultra-thin transition metal films, *Nat. Commun.* **5**, 4030 (2014).
- [13] O. Boule, J. Vogel, H. Yang, S. Pizzini, D. de Souza Chaves, A. Locatelli, T. Menteş, A. Sala, L. Buda-Prejbeanu, O. Klein *et al.*, Room-temperature chiral magnetic skyrmions in ultrathin magnetic nanostructures, *Nat. Nanotechnol.* **11**, 449 (2016).
- [14] S. Meyer, M. Perini, S. von Malottki, A. Kubetzka, R. Wiesendanger, K. von Bergmann, and S. Heinze, Isolated zero field sub-10 nm skyrmions in ultrathin Co films, *Nat. Commun.* **10**, 3823 (2019).
- [15] C. Moreau-Luchaire, C. Moutafis, N. Reyren, J. Sampaio, C. Vaz, N. Van Horne, K. Bouzehouane, K. Garcia, C. Deranlot, P. Warnicke *et al.*, Additive interfacial chiral interaction in multilayers for stabilization of small individual skyrmions at room temperature, *Nat. Nanotechnol.* **11**, 444 (2016).
- [16] A. Soumyanarayanan, M. Raju, A. Gonzalez Oyarce, A. Tan, M. Im, A. Petrovic, P. Ho, K. Khoo, M. Tran, C. Gan *et al.*, Tunable room-temperature magnetic skyrmions in Ir/Fe/Co/Pt multilayers, *Nat. Mater.* **16**, 898 (2017).
- [17] M. Raju, A. Yagil, A. Soumyanarayanan, A. K. Tan, A. Almoalem, F. Ma, O. Auslaender, and C. Panagopoulos, The evolution of skyrmions in Ir/Fe/Co/Pt multilayers and their topological Hall signature, *Nat. Commun.* **10**, 696 (2019).
- [18] M. Han, J. Garlow, Y. Liu, H. Zhang, J. Li, D. DiMarzio, M. W. Knight, C. Petrovic, D. Jariwala, and Y. Zhu, Topological magnetic-spin textures in two-dimensional van der Waals $\text{Cr}_2\text{Ge}_2\text{Te}_6$, *Nano Lett.* **19**, 7859 (2019).
- [19] B. Ding, Z. Li, G. Xu, H. Li, Z. Hou, E. Liu, X. Xi, F. Xu, Y. Yao, and W. Wang, Observation of magnetic skyrmion bubbles in a van der Waals ferromagnet Fe_3GeTe_2 , *Nano Lett.* **20**, 868 (2020).
- [20] J. Liang, W. Wang, H. Du, A. Hallal, K. Garcia, M. Chshiev, A. Fert, and H. Yang, Very large Dzyaloshinskii-Moriya interaction in two-dimensional Janus manganese dichalcogenides and its application to realize skyrmion states, *Phys. Rev. B* **101**, 184401 (2020).
- [21] C. Xu, J. Feng, S. Prokhorenko, Y. Nahas, H. Xiang, and L. Bellaiche, Topological spin texture in janus monolayers of the chromium trihalides $\text{Cr}(\text{I}, \text{X})_3$, *Phys. Rev. B* **101**, 060404(R) (2020).
- [22] W. Du, K. Dou, Z. He, Y. Dai, B. Huang, and Y. Ma, Spontaneous magnetic skyrmions in single-layer CrInX_3 ($\text{X} = \text{Te}, \text{Se}$), *Nano Lett.* **22**, 3440 (2022).
- [23] J. Liu, M. Shi, J. Lu, and M. P. Anantram, Analysis of electrical-field-dependent Dzyaloshinskii-Moriya interaction and magnetocrystalline anisotropy in a two-dimensional ferromagnetic monolayer, *Phys. Rev. B* **97**, 054416 (2018).
- [24] Y. Wu, S. Zhang, J. Zhang, W. Wang, Y. Zhu, J. Hu, G. Yin, K. Wong, C. Fang, C. Wan *et al.*, Néel-type skyrmion in $\text{WTe}_2/\text{Fe}_3\text{GeTe}_2$ van der Waals heterostructure, *Nat. Commun.* **11**, 3860 (2020).
- [25] T.-E. Park, L. Peng, J. Liang, A. Hallal, F. S. Yasin, X. Zhang, K. M. Song, S. J. Kim, K. Kim, M. Weigand *et al.*, Néel-type skyrmions and their current-induced motion in van der Waals ferromagnet-based heterostructures, *Phys. Rev. B* **103**, 104410 (2021).
- [26] Y. Wu, B. Francisco, Z. Chen, W. Wang, Y. Zhang, C. Wan, X. Han, H. Chi, Y. Hou, A. Lodesani *et al.*, A van der Waals interface hosting two groups of magnetic skyrmions, *Adv. Mater.* **34**, 2110583 (2022).
- [27] M. Yang, Q. Li, R. Chopdekar, R. Dhall, J. Turner, J. Carlström, C. Ophus, C. Klewe, P. Shafer, A. N'Diaye *et al.*, Creation of skyrmions in van der Waals ferromagnet Fe_3GeTe_2 on $(\text{Co}/\text{Pd})_n$ superlattice, *Sci. Adv.* **6**, eabb5157 (2020).
- [28] D. Li, S. Haldar, and S. Heinze, Strain-driven zero-field near-10 nm skyrmions in two-dimensional van der Waals heterostructures, *Nano Lett.* **22**, 7706 (2022).
- [29] D. Li, S. Haldar, T. Drevelow, and S. Heinze, Tuning the magnetic interactions in van der Waals Fe_3GeTe_2 heterostructures: A comparative study of ab initio methods, *Phys. Rev. B* **107**, 104428 (2023).
- [30] D. Li, S. Haldar, and S. Heinze, Proposal for all-electrical skyrmion detection in van der Waals tunnel junctions, *Nano Lett.* **24**, 2496 (2024).
- [31] Y. Gao, S. Yan, Q. Yin, H. Huang, Z. Li, Z. Zhu, J. Cai, B. Shen, H. Lei, Y. Zhang, and S. Wang, Manipulation of topological spin configuration via tailoring thickness in van der Waals ferromagnetic $\text{Fe}_{5-x}\text{GeTe}_2$, *Phys. Rev. B* **105**, 014426 (2022).
- [32] M. Schmitt, T. Denneulin, A. Kovács, T. G. Saunderson, P. Rüßmann, A. Shahee, T. Scholz, A. H. Tavabi, M. Gradhand, P. Mavropoulos *et al.*, Skyrmionic spin structures in layered Fe_5GeTe_2 up to room temperature, *Commun. Phys.* **5**, 254 (2022).
- [33] X. Lv, K. Pei, C. Yang, G. Qin, M. Liu, J. Zhang, and R. Che, Controllable topological magnetic transformations in the thickness-tunable van der Waals ferromagnet Fe_5GeTe_2 , *ACS Nano* **16**, 19319 (2022).
- [34] R. Fujita, P. Bassirian, Z. Li, Y. Guo, M. A. Mawass, F. Kronast, G. van der Laan, and T. Hesjedal, Layer-dependent magnetic domains in atomically thin Fe_5GeTe_2 , *ACS Nano* **16**, 10545 (2022).
- [35] B. W. Casas, Y. Li, A. Moon, Y. Xin, C. McKeever, J. Macy, A. K. Petford-Long, C. M. Phatak, E. J. Santos, E. S. Choi *et al.*, Coexistence of merons with skyrmions in the centrosymmetric van der Waals ferromagnet $\text{Fe}_{5-x}\text{GeTe}_2$, *Adv. Mater.* **35**, 2212087 (2023).
- [36] M. Högen, R. Fujita, A. K. C. Tan, A. Geim, M. Pitts, Z. Li, Y. Guo, L. Stefan, T. Hesjedal, and M. Atatüre, Imaging nucleation and propagation of pinned domains in few-layer $\text{Fe}_{5-x}\text{GeTe}_2$, *ACS Nano* **17**, 16879 (2023).
- [37] A. F. May, D. Ovchinnikov, Q. Zheng, R. Hermann, S. Calder, B. Huang, Z. Fei, Y. Liu, X. Xu, and M. A. McGuire, Ferromagnetism near room temperature in the cleavable van der Waals crystal Fe_5GeTe_2 , *ACS Nano* **13**, 4436 (2019).

- [38] H. Zhang, R. Chen, K. Zhai, X. Chen, L. Caretta, X. Huang, R. V. Chopdekar, J. Cao, J. Sun, J. Yao *et al.*, Itinerant ferromagnetism in van der Waals $\text{Fe}_{5-x}\text{GeTe}_2$ crystals above room temperature, *Phys. Rev. B* **102**, 064417 (2020).
- [39] S. von Malottki, B. Dupé, P. Bessarab, A. Delin, and S. Heinze, Enhanced skyrmion stability due to exchange frustration, *Sci. Rep.* **7**, 12299 (2017).
- [40] S. Haldar, S. von Malottki, S. Meyer, P. F. Bessarab, and S. Heinze, First-principles prediction of sub-10-nm skyrmions in Pd/Fe bilayers on Rh(111), *Phys. Rev. B* **98**, 060413(R) (2018).
- [41] S. Paul, S. Haldar, S. von Malottki, and S. Heinze, Role of higher-order exchange interactions for skyrmion stability, *Nat. Commun.* **11**, 4756 (2020).
- [42] Welcome to the FLEUR-project, www.flapw.de (accessed Sept. 1, 2022).
- [43] See Supplemental Material at <http://link.aps.org/supplemental/10.1103/PhysRevB.109.L220404> for computational details, spin-resolved DOS for the monolayer Fe_5GeTe_2 , spin spiral calculations without SOC for the FGT family, spin moment with respect to \mathbf{q} for the Fe_5GeTe_2 monolayer, Monte Carlo simulations, the zero-temperature phase diagram for monolayer Fe_5GeTe_2 , as well as spin spiral curves for conical spin spirals, and which includes Refs. [40,42,44,46–51,59–65].
- [44] P. Kurz, F. Förster, L. Nordström, G. Bihlmayer, and S. Blügel, *Ab initio* treatment of noncollinear magnets with the full-potential linearized augmented plane wave method, *Phys. Rev. B* **69**, 024415 (2004).
- [45] M. Heide, G. Bihlmayer, and S. Blügel, Describing Dzyaloshinskii-Moriya spirals from first principles, *Phys. B* **404**, 2678 (2009).
- [46] X. Yang, X. Zhou, W. Feng, and Y. Yao, Strong magneto-optical effect and anomalous transport in the two-dimensional van der Waals magnets Fe_nGeTe_2 ($n = 3, 4, 5$), *Phys. Rev. B* **104**, 104427 (2021).
- [47] S. Ershadrad, S. Ghosh, D. Wang, Y. Kvashnin, and B. Sanyal, Unusual magnetic features in two-dimensional Fe_5GeTe_2 induced by structural reconstructions, *J. Phys. Chem. Lett.* **13**, 4877 (2022).
- [48] S. Ghosh, S. Ershadrad, V. Borisov, and B. Sanyal, Unraveling effects of electron correlation in two-dimensional Fe_nGeTe_2 ($n = 3, 4, 5$) by dynamical mean field theory, *Npj Comput. Mater.* **9**, 86 (2023).
- [49] P. Bessarab, V. Uzdin, and H. Jónsson, Method for finding mechanism and activation energy of magnetic transitions, applied to skyrmion and antivortex annihilation, *Comput. Phys. Commun.* **196**, 335 (2015).
- [50] P. F. Bessarab, G. P. Müller, I. S. Lobanov, F. N. Rybakov, N. S. Kiselev, H. Jónsson, V. M. Uzdin, S. Blügel, L. Bergqvist, and A. Delin, Lifetime of racetrack skyrmions, *Sci. Rep.* **8**, 3433 (2018).
- [51] S. von Malottki, P. F. Bessarab, S. Haldar, A. Delin, and S. Heinze, Skyrmion lifetime in ultrathin films, *Phys. Rev. B* **99**, 060409(R) (2019).
- [52] F. Muckel, S. von Malottki, C. Holl, B. Pestka, M. Pratzner, P. Bessarab, S. Heinze, and M. Morgenstern, Experimental identification of two distinct skyrmion collapse mechanisms, *Nat. Phys.* **17**, 395 (2021).
- [53] Note, that the dipole-dipole interaction also prefers an in-plane magnetization direction as the MAE. For monolayer Fe_5GeTe_2 its energy contribution amounts to about 60% of the MAE. If we include the dipolar energy, the critical magnetic field required to obtain the field-polarized phase with an out-of-plane magnetization increases to about 3.4 T.
- [54] A. Bocdanov and A. Hubert, The properties of isolated magnetic vortices, *Phys. Status Solidi (b)* **186**, 527 (1994).
- [55] C. Tan, J. Lee, S. Jung, T. Park, S. Albarakati, J. Partridge, M. Field, D. McCulloch, L. Wang, and C. Lee, Hard magnetic properties in nanoflake van der Waals Fe_3GeTe_2 , *Nat. Commun.* **9**, 1554 (2018).
- [56] Y. Wang, X. Chen, and M. Long, Modifications of magnetic anisotropy of Fe_3GeTe_2 by the electric field effect, *Appl. Phys. Lett.* **116**, 092404 (2020).
- [57] S. Park, D. Kim, Y. Liu, J. Hwang, Y. Kim, W. Kim, J. Kim, C. Petrovic, C. Hwang, S. Mo, H. Kim, B. Min, H. Koo, J. Chang, C. Jang, J. Choi, and H. Ryu, Controlling the magnetic anisotropy of the van der Waals ferromagnet Fe_3GeTe_2 through hole doping, *Nano Lett.* **20**, 95 (2020).
- [58] A. S. Varentcova, S. von Malottki, M. N. Potkina, G. Kwiatkowski, S. Heinze, and P. F. Bessarab, Toward room-temperature nanoscale skyrmions in ultrathin films, *npj Comput. Mater.* **6**, 193 (2020).
- [59] P. Giannozzi, S. Baroni, N. Bonini, M. Calandra, R. Car, C. Cavazzoni, D. Ceresoli, G. L. Chiarotti, M. Cococcioni, I. Dabo *et al.*, QUANTUM ESPRESSO: A modular and open-source software project for quantum simulations of materials, *J. Phys.: Condens. Matter* **21**, 395502 (2009).
- [60] H. L. Zhuang, P. R. C. Kent, and R. G. Hennig, Strong anisotropy and magnetostriction in the two-dimensional stoner ferromagnet Fe_3GeTe_2 , *Phys. Rev. B* **93**, 134407 (2016).
- [61] Y. Deng, Y. Yu, Y. Song, J. Zhang, N. Wang, Z. Sun, Y. Yi, Y. Wu, S. Wu, J. Zhu *et al.*, Gate-tunable room-temperature ferromagnetism in two-dimensional Fe_3GeTe_2 , *Nature (London)* **563**, 94 (2018).
- [62] M. Joe, U. Yang, and C. Lee, First-principles study of ferromagnetic metal Fe_5GeTe_2 , *Nano Mater. Sci.* **1**, 299 (2019).
- [63] J. Mentink, M. Tretyakov, A. Fasolino, M. Katsnelson, and T. Rasing, Stable and fast semi-implicit integration of the stochastic Landau–Lifshitz equation, *J. Phys.: Condens. Matter* **22**, 176001 (2010).
- [64] J. Alzate-Cardona, D. Sabogal-Suárez, R. Evans, and E. Restrepo-Parra, Optimal phase space sampling for monte carlo simulations of Heisenberg spin systems, *J. Phys.: Condens. Matter* **31**, 095802 (2019).
- [65] M. Böttcher, S. Heinze, S. Egorov, J. Sinova, and B. Dupé, B - T phase diagram of Pd/Fe/Ir (111) computed with parallel tempering Monte Carlo, *New J. Phys.* **20**, 103014 (2018).

Supplemental Material: Prediction of stable nanoscale skyrmions in monolayer Fe_5GeTe_2

Dongzhe Li,^{1,*} Soumyajyoti Haldar,² Leo Kollwitz,² Hendrik Schrautzer,^{2,3} Moritz A. Goerzen,² and Stefan Heinze^{2,4}

¹*CEMES, Université de Toulouse, CNRS, 29 rue Jeanne Marvig, F-31055 Toulouse, France*

²*Institute of Theoretical Physics and Astrophysics, University of Kiel, Leibnizstrasse 15, 24098 Kiel, Germany*

³*Science Institute and Faculty of Physical Sciences, University of Iceland, VR-III, 107 Reykjavik, Iceland*

⁴*Kiel Nano, Surface, and Interface Science (KiNSIS), University of Kiel, Germany*

(Dated: May 24, 2024)

I. Density functional theory calculations

A. Structural relaxations

For the atomic relaxation, we employed the generalized gradient approximation (GGA) using the QUANTUM ESPRESSO [1] code. We obtained a relaxed lattice constant of 3.96 Å for Fe_5GeTe_2 , which is in good agreement with the previous study [2]. Energy cut-offs of 45 Ry and 450 Ry were employed for the wavefunctions and the charge density, respectively. The Brillouin-zone has been discretized by using a $(16 \times 16 \times 1)$ \mathbf{k} -points mesh. In addition, a vacuum space of about 30 Å was taken to separate two neighboring slabs in the z direction (perpendicular to the surface) in order to avoid unphysical interactions.

B. Spin spiral calculations

For magnetic exchange calculations, we used the local density approximation (LDA) without Hubbard U correction since it yields a magnetic moment of $1.76 \mu_B/\text{Fe}$ that compares well with experiments, as also pointed out in Ref. [3, 4]. For spin spiral calculations, we employed the full-potential linearized augmented plane wave method (FLAPW) as implemented in the FLEUR code [5] based on the generalized Bloch theorem (gBT) [6]. It allows considering spin-spirals of any wave-vector \mathbf{q} for systems without SOC. We first self-consistently compute the energy dispersion of homogeneous flat spin spirals curve, $E_{ss}(\mathbf{q})$, which are characterized by a wave vector \mathbf{q} and an angle $\phi = \mathbf{q} \cdot \mathbf{R}$ between adjacent magnetic moments separated by lattice vector \mathbf{R} . As a next step, the DMI will be computed within the first-order perturbation theory on the self-consistent spin spiral state. We used a cutoff parameter for FLAPW basis functions of $K_{\max} = 4.0 \text{ a.u.}^{-1}$, and we included basis functions including spherical harmonics up to $l_{\max} = 8$. To extract J_{ij} and \mathbf{D}_{ij} parameters, we converge the total energy of flat spin-spiral states (without SOC and with SOC using force theorem) using a $33 \times 33 \times 1$ \mathbf{k} -point mesh in order to obtain an accuracy of 0.001 meV. Since magnetic moments on Fe atoms vary with increasing \mathbf{q} vector, we also compared our spin spiral curves for flat spin spirals to conical spin spirals. For the conical spin spirals, we chose an angle $\theta = \pi/20$. To facilitate a direct comparison with the

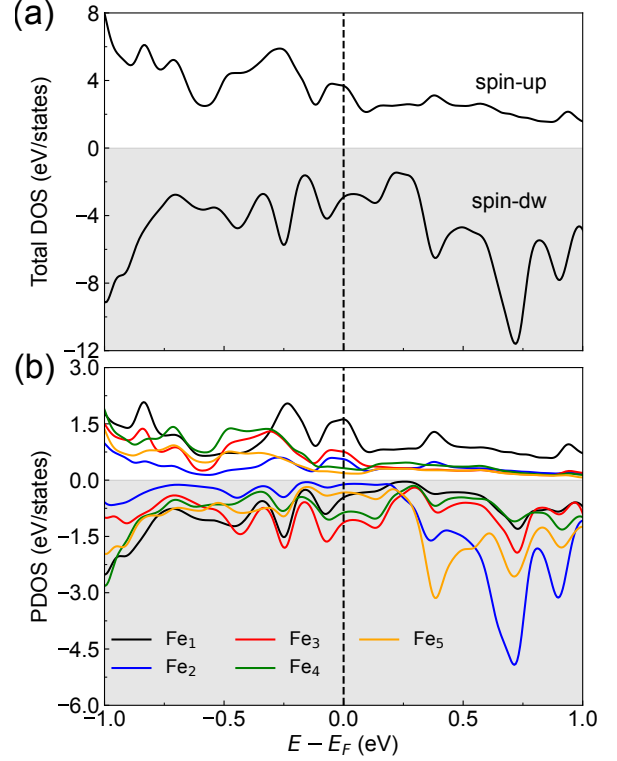


Figure S 1. (a) Spin-resolved total density of states (DOS) for the F5GT monolayer. (b) Spin-resolved projected DOS on different magnetic Fe atoms.

energy dispersion of flat spin spirals, we re-scaled the energies of the conical spin spirals by $1/\sin^2 \theta$. Since the energy differences around the Γ point are very small, we increased K_{\max} to 4.3 a.u.^{-1} and used a denser \mathbf{k} -mesh of 66×66 .

The magnetic anisotropy energy (MAE) was calculated using the force theorem, where the band energies for in-plane (E_{\parallel}) and out-of-plane (E_{\perp}) directions are obtained after a single diagonalization of the Hamiltonian including SOC, but starting from self-consistently converged charge densities of scalar-relativistic calculations. The uniaxial anisotropy is determined using $K = E_{\perp} - E_{\parallel}$. We used a very dense \mathbf{k} -point mesh of 87×87 in the full two-dimensional BZ. All calculations were done in the local density approximation (LDA).

* dongzhe.li@cemes.fr

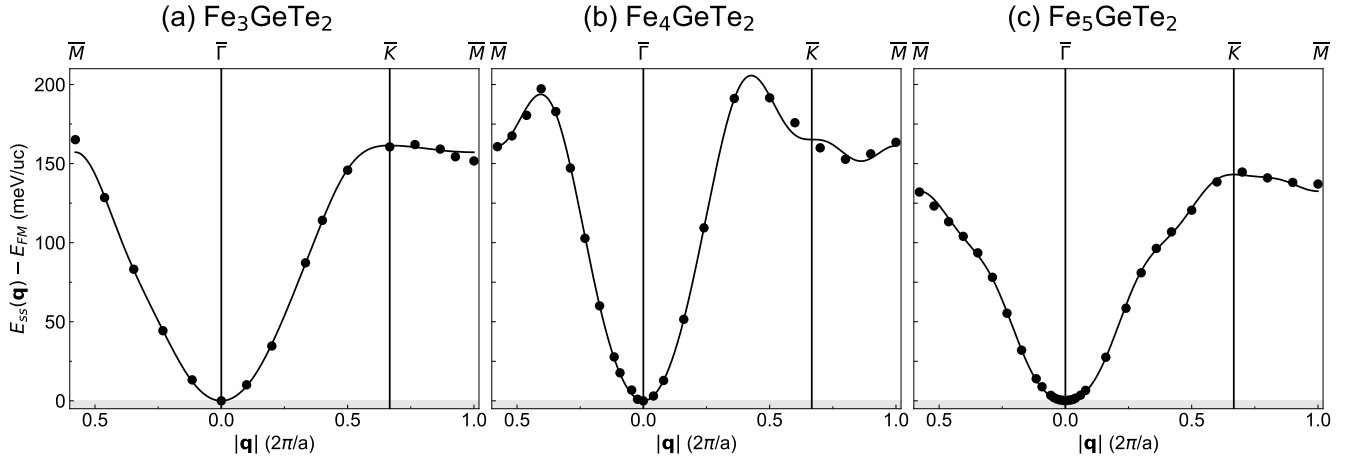


Figure S 2. Energy dispersion $E_{SS}(\mathbf{q})$ with respect to the FM state, E_{FM} , of flat cycloidal spin spirals for the Fe_3GeTe_2 (a), Fe_4GeTe_2 (b), Fe_5GeTe_2 (c) monolayers along the high symmetry path $\bar{M}-\bar{\Gamma}-\bar{K}-\bar{M}$ without SOC. The symbols represent the DFT calculations in scalar-relativistic approximation, while the solid lines are the fits to the Heisenberg exchange interaction.

	J_1	J_2	J_3	J_4	J_5	J_6	J_7	J_8	K	inversion symmetry	no of Fe atoms
Fe_3GeTe_2	19.28	-0.77	-1.25	0.08	1.11	-0.39	-0.04	-0.11	-3.01	Yes	3
Fe_4GeTe_2	15.61	9.27	6.34	-2.38	-1.55	-0.15	0.79	-0.42	3.03	Yes	4
Fe_5GeTe_2	14.80	0.89	0.46	0.91	0.23	-0.44	-0.59	0.00	0.38	No	5

Table S I. Shell-resolved Heisenberg interaction constants (J_i) obtained via DFT for the FGT family monolayer. A positive (negative) sign represents a ferromagnetic (antiferromagnetic) coupling. We also added MAE values, where positive values indicate out-of-plane magnetization, and negative values correspond to in-plane magnetization. Note that, in our spin model, since we are treating 3, 4, or 5 Fe atoms as a whole system for Fe_3GeTe_2 , Fe_4GeTe_2 , Fe_5GeTe_2 , the physical meaning of different parameters is more complex. For instance, our J_1 cannot be interpreted as one NN Fe-Fe pair interaction but contains all different NN interactions between 5 Fe atoms, contributing in an averaged way. All values are given in meV/unit cell.

	Fe_1	Fe_2	Fe_3	Fe_4	Fe_5	\bar{m}_{Fe}
GGA [7, 8]	0.11	2.30	2.04	1.46	2.57	1.70
GGA [9]	0.10	2.27	2.07	1.48	2.56	1.65
GGA+DMFT [8]	-0.14	2.40	1.95	1.31	2.63	1.63
LDA (this work)	-0.27	2.21	1.70	1.28	2.41	1.46

Table S II. Comparison of calculated spin moments on different Fe atoms (see Fig. 1 in the main text for the atom notation) and average magnetic moments of monolayer Fe_5GeTe_2 (in μ_B) using different levels of theory, namely DFT with GGA [7–9] or LDA functionals or dynamical mean-field theory (DMFT) [8].

II. Atomistic spin simulations

In order to relax isolated skyrmions in the ferromagnetic background, we performed spin dynamics simulations based on the Landau–Lifshitz equation:

$$\hbar \frac{d\mathbf{m}_i}{dt} = \frac{\partial H}{\partial \mathbf{m}_i} \times \mathbf{m}_i - \alpha \left(\frac{\partial H}{\partial \mathbf{m}_i} \times \mathbf{m}_i \right) \times \mathbf{m}_i \quad (1)$$

where \hbar , α , and H are the reduced Planck constant, the damping parameter, and the Hamiltonian in Eq. (1) in the main text. We solve Eq. 1 using a SIB solver proposed by Mentink *et al.* [10]. For all spin dynamics simulations, we used a damping parameter of $\alpha = 0.05$ and a system size of 100×100 atoms on a hexagonal lattice with periodic boundary condi-

tions.

A. Geodesic nudged elastic band method

First of all, we created isolated skyrmions in the FM background and relaxed the spin structure using spin dynamics by applying a magnetic field above the critical magnetic field (B_c) from the theoretical profile. After that, using the GNEB method [11], we calculated the skyrmion collapse, and the maximum along a minimum energy path corresponds to the first-order saddle point on the energy surface. The first and last images were chosen as skyrmion and FM states, respectively. The intermediate images were achieved by a force projection scheme. To ensure uniform distribution of the images along the path, we calculated the effective field at each image, and its local tangent to the path was replaced by a spring force. Finally, the saddle point (which corresponds to the energy barrier separating two stable states) was computed using a climbing image method on top of GNEB.

It is worth noting that we assume in our spin model that constant magnetic moments in our atomistic spin simulations. However, the magnetic moments on different Fe atoms change for non-collinear spin states as shown by our DFT spin spiral calculations when we increase \mathbf{q} (Fig. S3). To check that this will not change our general conclusions, we have also per-

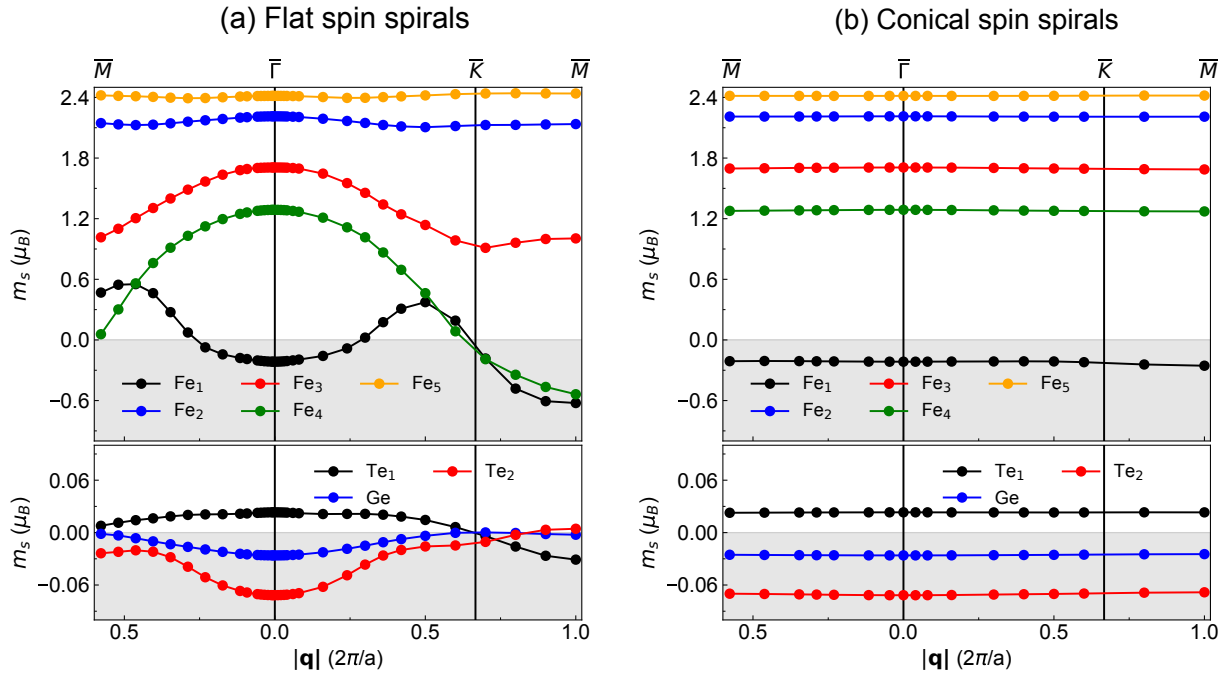


Figure S 3. (a) Magnetic moments variation along the high-symmetry direction $\bar{M}\text{-}\bar{\Gamma}\text{-}\bar{K}\text{-}\bar{M}$ for different atoms for flat spin spirals. (b) The same as (a) but for conical spin spirals with $\theta = \pi/20$.

formed conical spin spiral calculations where we have constant spin moments. Our DFT calculations indicate that the energies of both conical and flat spin spirals align almost perfectly near the $\bar{\Gamma}$ point for DMI (see Fig. S4). Since the DMI is the main contribution that stabilizes skyrmions against collapse for Fe_5GeTe_2 , the energy barriers will not change significantly either if our spin model does not perfectly capture the exchange frustration compared to conical spin spirals.

B. Skyrmion lifetime by harmonic transition state theory

In transition state theory the average lifetime τ of a magnetic state takes the form of an Arrhenius law

$$\tau = f_0^{-1} \exp\left(\frac{\Delta E}{k_B T}\right) \quad (2)$$

here, ΔE corresponds to an energy barrier between the initial and final state which is extracted from the minimum energy path calculated with GNEB. The pre-factor for skyrmion lifetime f_0 takes the form [12–14]

$$f_0 = \frac{2\lambda k_B T}{L} \frac{\prod_i \sqrt{\epsilon_{\text{sk},i}}}{\prod_i \sqrt{\epsilon_{\text{sp},i}}} \quad (3)$$

where the dynamical factor λ , the hessian eigenvalues $\epsilon_{\text{sp},i}$, $\epsilon_{\text{sk},i}$ at the skyrmion (sk) and saddle point (sp) as well as the zero mode partition function L are computed as a function of external fields and temperature. Note that the products run only over eigenvalues $\epsilon_i > 0$ while zero modes with $\epsilon_i \approx 0$,

which in our case are only the translations of the skyrmion, are treated effectively in L and the unstable mode at the sp with $\epsilon_{\text{sp},1} < 0$ is omitted.

III. Monte-Carlo simulations

For the Monte-Carlo (MC) simulation, an adaptive single spin sampling algorithm [15] with Metropolis acceptance probability

$$p(\mathbf{M} \rightarrow \mathbf{M}') = \min[1, \exp(-\beta(E(\mathbf{M}') - E(\mathbf{M})))] \quad (4)$$

within the extended Heisenberg model (Eq. (1) in the main text) was used. The full and effective models with parameters given in Tab. 1 in the main text are investigated. The initial simulation starts from a random configuration at $T_{\text{ini}} = 1000$ K and is cooled down to $T_{\text{fin}} = 1$ K. We performed 4000 MC cycles at each temperature in order to equilibrate the system, with each cycle consisting of N^2 single spin updates for an $N \times N \times 1$ lattice. The thermodynamic averages are calculated across 10000 MC cycles. This was done for the different lattice sizes up to $80 \times 80 \times 1$ to investigate finite size effects, which have a negligible influence on the largest systems compared to the statistical error.

For the $80 \times 80 \times 1$ lattice with periodic boundary conditions, the simulation was repeated with a finer temperature sampling with 1000 MC cycles for the equilibration and 40000 MC cycles for the averaging at each temperature. The results can be seen in Fig. S 5. The specific heat c_V derived

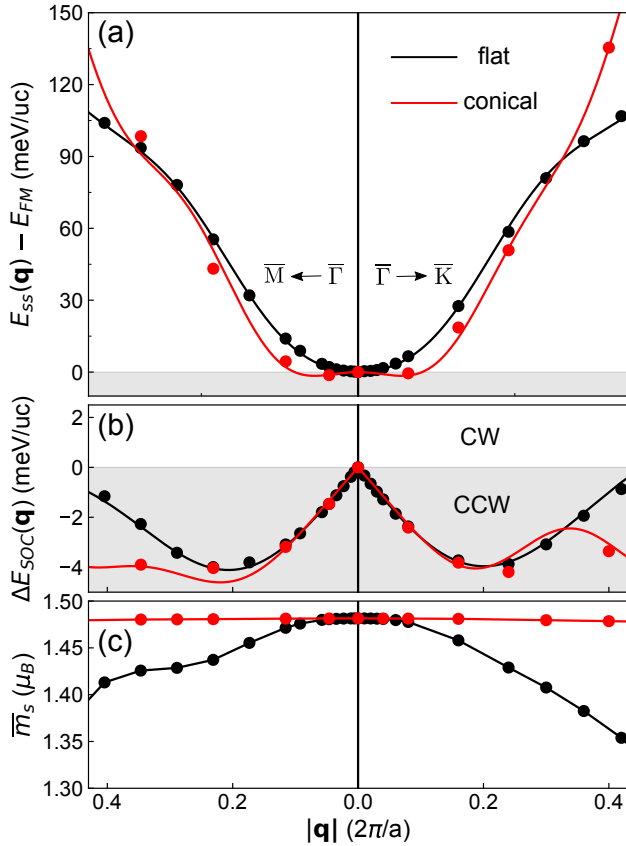


Figure S 4. (a) Energy dispersions $E(\mathbf{q})$ without SOC comparing flat cycloidal spin spirals for Fe_5GeTe_2 with conical spin spiral states. (b) The same as (a) but for the energy contribution due to DMI. (c) The averaged spin moment on Fe atoms long the high-symmetry directions.

from the total energy E of the system is calculated via [16]

$$c_V = \frac{1}{k_B T^2} (\langle E^2 \rangle - \langle E \rangle^2). \quad (5)$$

It exhibits a maximum indicating a phase transition. The temperature at which this maximum occurs marks the transition temperature T_c . It was determined by fitting the function

$$c_V^{\text{fit}}(T) = A|T - T_c|^\epsilon + C \quad (6)$$

with fit parameters A , ϵ , C . The dashed line in Fig. S 5(a) marks the transition temperature for the full model while the dotted line shows T_c for the effective model, which was determined in the same way. For the full model we obtain $T_c = 451$ K and for the effective model $T_c = 424$ K.

Fig. S 5(b) and (c) show the temperature dependence of the total magnetization for the full and effective model, respectively, with the transition temperatures determined from the specific heat shown by lines. The two spin models behave qualitatively different. The magnetization of the full spin model system goes to zero for low temperatures, as this system relaxes into a spin spiral state; the magnetization of the effective spin model system tends towards unity, as here a ferromagnetic ground state is realized due to the in-plane MAE. The ground state of the full model mainly consists of a spin spiral with a period of 26.4 nm. This is larger than the period of the spin spiral minimum and is due to the lattice dimension of $80 \times 80 \times 1$ being incommensurable with the 19.9 nm period of the spin spiral minimum. For a nearly commensurable lattice dimension of $50 \times 50 \times 1$ the period of the spin spiral ground state is equivalent to the one of the spin spiral minimum (see Fig. 2c in the main text). The vanishing of the total magnetization for the full model leads to large statistical errors, which makes it unsuitable as an order parameter. For this reason we resorted to the heat capacity in order to determine the transition temperatures. MC simulations were also carried out without the inclusion of the DMI. This leads to a ferromagnetic ground state for both the full and the effective spin model but only results in small deviations of less than 5 K in the transition temperatures.

The transition temperatures obtained from our MC simulations are in reasonable agreement with the value of $T_c = 390$ K obtained in Ref. [7], considering the vastly different spin models with interaction constants obtained based on different DFT codes. The treatment of the system as an effective monolayer in our spin model results in a slight overestimation of the thermal stability compared to the explicit treatment of the spins of all Fe layers of Ref. [7]. However, the small deviation of the transition temperatures shows that the spins of the separate Fe layers are strongly exchange coupled, as assumed in our spin model. This is also supported by the explicit inter-layer exchange constants reported in Ref. [7].

[1] P. Giannozzi, S. Baroni, N. Bonini, M. Calandra, R. Car, C. Cavazzoni, D. Ceresoli, G. L. Chiarotti, M. Cococcioni, I. Dabo, et al., *J. Phys. Condens. Matter* **21**, 395502 (2009).
 [2] X. Yang, X. Zhou, W. Feng, and Y. Yao, *Phys. Rev. B* **104**, 104427 (2021).
 [3] H. Zhuang, P. Kent, and R. Hennig, *Phys. Rev. B* **93**, 134407 (2016).
 [4] Y. Deng, Y. Yu, Y. Song, J. Zhang, N. Wang, Z. Sun, Y. Yi, Y. Wu, S. Wu, J. Zhu, et al., *Nature* **563**, 94 (2018).
 [5] *Welcome to the FLEUR-project*, www.flapw.de (accessed Sept.

1, 2022).
 [6] P. Kurz, F. Förster, L. Nordström, G. Bihlmayer, and S. Blügel, *Phys. Rev. B* **69**, 024415 (2004).
 [7] S. Ershadrad, S. Ghosh, D. Wang, Y. Kvashnin, and B. Sanyal, *J. Phys. Chem. Lett.* **13**, 4877 (2022).
 [8] S. Ghosh, S. Ershadrad, V. Borisov, and B. Sanyal, *Npj Comput. Mater.* **9**, 86 (2023).
 [9] M. Joe, U. Yang, and C. Lee, *Nano Mater. Sci.* **1**, 299 (2019).
 [10] J. Mentink, M. Tretyakov, A. Fasolino, M. Katsnelson, and T. Rasing, *J. Phys. Condens. Matter* **22**, 176001 (2010).

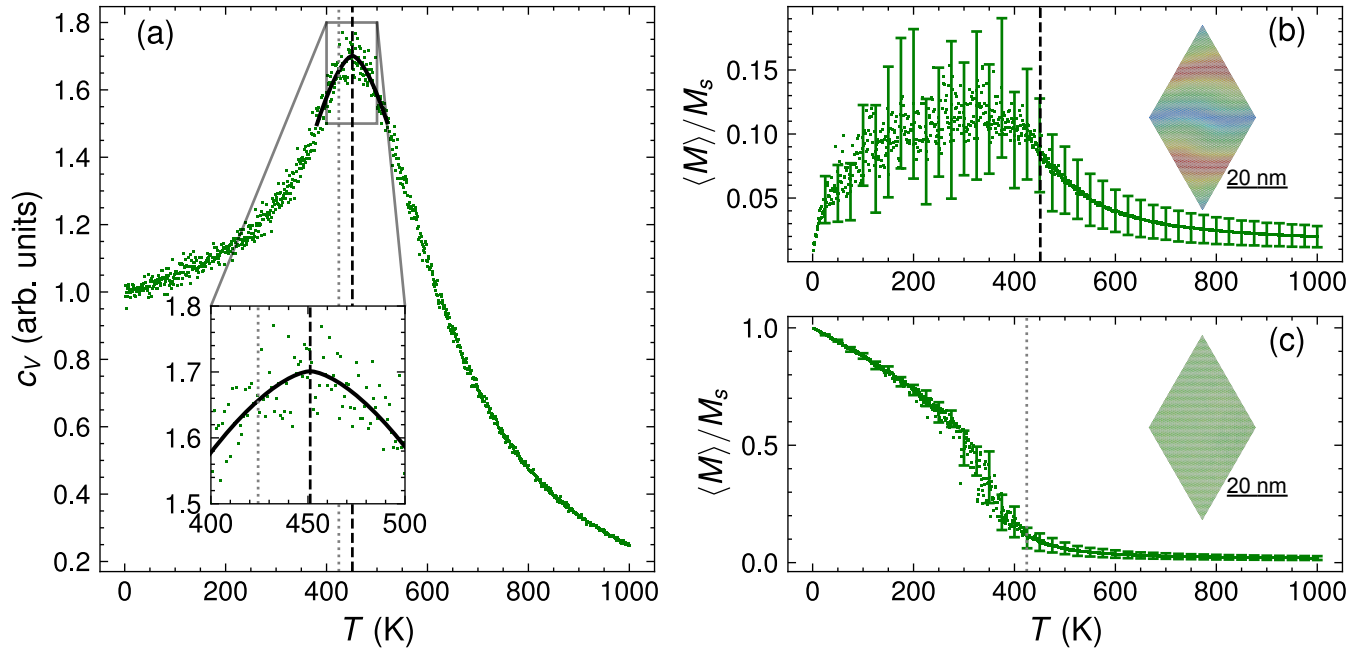


Figure S 5. (a) Temperature dependence of the specific heat c_V for the full model parameters on an $80 \times 80 \times 1$ lattice. The dashed line (black) shows the transition temperature occurring at the maximum of the fitted data. The dotted line (grey) shows the transition temperature of the effective model which was determined analogously. The inset shows a zoomed in view of the maximum of the specific heat. (b) and (c) Temperature dependence of the magnetization for the full and effective model, respectively. For the full model, the magnetization vanishes for low temperatures as the systems exhibit a spin spiral ground state, while for the effective model, a ferromagnetic state (in-plane) is realized in agreement with the DFT calculations. The insets show the respective system at $T = 1$ K.

- [11] P. Bessarab, V. Uzdin, and H. Jónsson, *Comput. Phys. Commun.* **196**, 335 (2015).
- [12] S. Haldar, S. von Malottki, S. Meyer, P. Bessarab, and S. Heinze, *Phys. Rev. B* **98**, 060413 (2018).
- [13] S. von Malottki, P. Bessarab, S. Haldar, A. Delin, and S. Heinze, *Phys. Rev. B* **99**, 060409 (2019).
- [14] P. F. Bessarab, G. P. Müller, I. S. Lobanov, F. N. Rybakov, N. S. Kiselev, H. Jónsson, V. M. Uzdin, S. Blügel, L. Bergqvist, and A. Delin, *Sci. Rep.* **8**, 1 (2018).
- [15] J. Alzate-Cardona, D. Sabogal-Suárez, R. Evans, and E. Restrepo-Parra, *Journal of Physics: Condensed Matter* **31**, 095802 (2019).
- [16] M. Böttcher, S. Heinze, S. Egorov, J. Sinova, and B. Dupé, *New Journal of Physics* **20**, 103014 (2018).

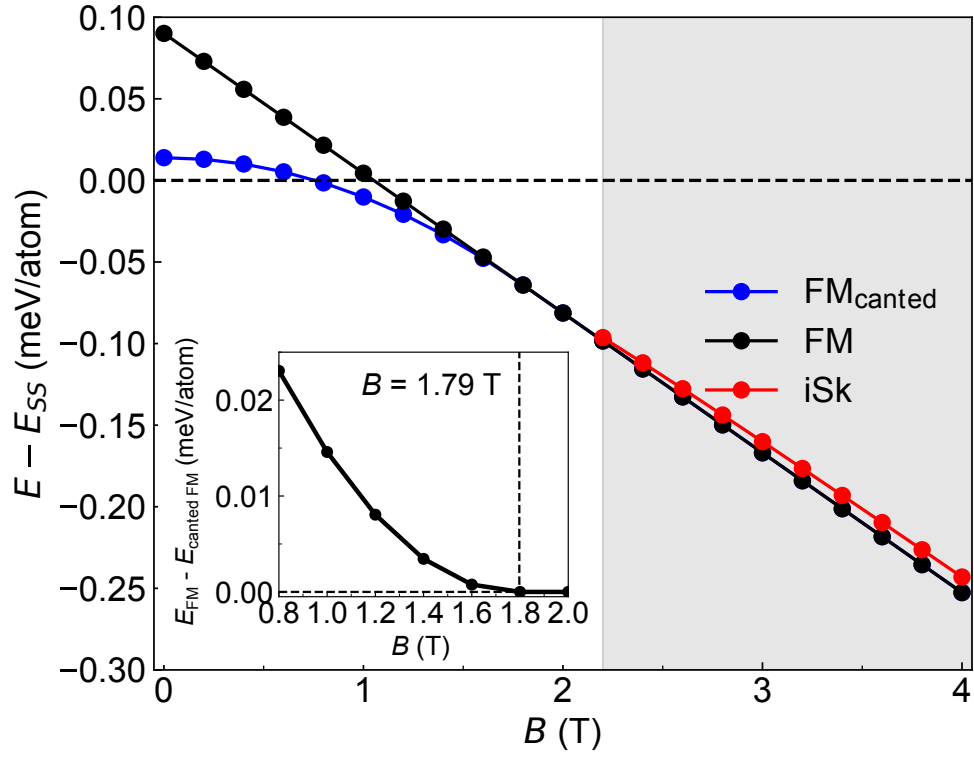


Figure S 6. Zero temperature phase diagram for Fe_5GeTe_2 based on DFT parameters for the magnetic interactions. The energies of the isolated skyrmion (iSk), canted ferromagnetic (FM_{canted}), and out-of-plane ferromagnetic (FM) states are plotted with respect to the homogeneous spin spiral (zero dotted line). The black-filled region represents the regime where isolated skyrmions become metastable in the FM (out-of-plane) background. The inset shows the energy difference between the out-of-plane FM state and the canted FM state with an angle with respect to the surface normal, which depends on B .